ELSEVIER

Contents lists available at ScienceDirect

Journal of Membrane Science

journal homepage: www.elsevier.com/locate/memsci



Porous hydrophobic-hydrophilic composite membranes for direct contact membrane distillation



Aishwarya A. Puranik, Lydia N. Rodrigues, John Chau, Lin Li¹, Kamalesh K. Sirkar*

Otto York Department of Chemical, Biological and Pharmaceutical Engineering, New Jersey Institute of Technology, University Heights, Newark, NJ, 07102, USA

ARTICLE INFO

Keywords: Membrane distillation Composite membrane Plasma-polymerized hydrophobic fluorosiloxane coating Hydrophilic porous substrate Stacked composite membrane

ABSTRACT

Direct contact membrane distillation (DCMD) for desalination is attractive for high salt concentrations if low-cost steam/waste heat is available and waste brine disposal cost for inland desalination is factored in. A number of innovations have taken place in DCMD in terms of the structure of the porous hydrophobic membrane. Composite membranes are of increasing interest. Composite membrane structures of great interest include a thin hydrophobic porous layer over a porous hydrophilic layer of polyvinylidene fluoride (PVDF) or a thin porous hydrophobic layer over a more conventional hydrophobic porous membrane. These membranes can be in the form of an integral composite or a stacked composite or a laminated composite. A facile method of fabricating such integral composite membranes is plasma polymerization under vacuum. A class of such membranes yielding quite high water vapor fluxes have been characterized using a variety of characterization techniques: Contact angle, liquid entry pressure (LEP), bubble-point pressure, scanning electron microscopy (SEM), energy-dispersive X-ray spectroscopy (EDS), atomic force microscopy (AFM). Stacked composites of a hydrophobic ePTFE membrane over a hydrophobiic PVDF membrane or a hydrophobic PVDF membrane over another hydrophobic PVDF membrane were also studied. Novel conditions created lead to very high water vapor fluxes compared to those from conventional hydrophobic membranes supported on a mesh support.

1. Introduction

Membrane Distillation (MD) is an evaporation process for a volatile solvent or solute species from a solution. It is often investigated for desalination. Various MD methods studied include Direct Contact Membrane Distillation (DCMD), Vacuum Membrane Distillation (VMD), Sweep Gas Membrane Distillation (SGMD) and Air Gap Membrane Distillation (AGMD). DCMD is the most common type of membrane distillation method studied. Earliest membranes investigated for DCMD were commercially available porous hydrophobic polymeric membranes from polymers such as polypropylene (PP), polyvinylidene fluoride (PVDF) and polytetrafluoroethylene (PTFE) and used for microfiltration processes.

The membrane distillation process of DCMD for desalination imposes certain requirements on the porous membrane and the feed and permeate solutions. These include high water vapor flux, no salt leakage, high liquid entry pressure, reduced conductive heat loss, high thermal efficiency, reduced temperature polarization, prevention of membrane fouling and high gained output ratio (GOR). Some of these requirements act at cross-purposes. For example, a thinner hydrophobic

membrane yields higher fluxes but reduces thermal efficiency considerably [1]. However, if the temperature difference between the two sides of the membrane are lowered to 10–20 °C, the thermal efficiency values can be high [2]. This is one way for DCMD thermal efficiency to be around 85% [2] compared to 95–99% + thermal efficiency values achieved in VMD process [3–7].

A thin porous hydrophobic membrane capable of yielding high flux needs a mechanical support. Alternately, one can create a thin hydrophobic layer on a porous hydrophilic support by polymer coating, polymer grafting, plasma polymerization (originally suggested by Cheng and Wiersma [8]), and using fluorinated surface modifying hydrophobic macromolecules during hydrophilic membrane casting (Khayet et al. [9–11], [12]). Dual-layer hydrophobic–hydrophilic hollow fiber membranes of hydrophobic PVDF outside layer and inner hydrophilic layer filled with high thermal conductivity additives were developed and modeled [13]. Performances of a flat thin hydrophobic PTFE membrane supported on a hydrophobic scrim-backing PP support layer have been studied and modeled [14].

Prevention of membrane fouling in DCMD, especially when scaling salts precipitate due to high water recovery, is also an item of

E-mail address: sirkar@njit.edu (K.K. Sirkar).

^{*} Corresponding author.

¹ Current address: Fordoz Pharma, East Windsor, NJ USA.

considerable concern. To achieve such a goal, a very thin highly porous hydrophobic fluorosiloxane coating was developed on the outer surface of thick porous hydrophobic PP hollow fibers by plasma polymerization [15–17]. With hot brine in cross flow across the outside of these coated hollow fibers, it was demonstrated that the near-superhydrophobic membrane surface (contact angle $\sim 140^\circ$) was not fouled and the flux remained unaffected even though scaling salt precipitates were floating all around [16,18].

There are a number of studies where plasma polymerization was used to modify the surface of porous hydrophobic membranes and create composite hydrophobic-hydrophobic structures with the goal of creating a more hydrophobic surface to prevent pore wetting. Yang et al. [19] modified the surface of flat-sheet porous hydrophobic GVHP type PVDF membranes using CF4 plasma. This group has made a number of related studies. Chen et al. [20] developed negatively charged superhydrophobic membrane surface via plasma surface treatment of PVDF membranes to develop anti-wetting behavior in DCMD. Tijing et al. [21] developed superhydrophobic nanofiber membranes for DCMD by electrospinning PVDF-co-PCH and incorporating carbon nanotubes. Lee et al. [22] incorporated fluorosilanecoated TiO₂ nanocomposites in electrospun nanofibers to develop DCMD membranes with somewhat better performance. By CF₄ plasma modification, Tian et al. [23] converted hydrophilic polysulfone membrane blended with polyvinyl pyrolidone into a hydrophobic membrane. Jeong et al. [24] modified hydrophobic PVDF membrane surfaces by O2 and CF4 plasma treatment.

There has also been a significant effort to develop a thin hydrophobic coating on porous hydrophilic membrane surfaces (following [9-13]) by plasma coating and other methods. Wei et al. [25] used CF₄ plasma treatment to develop a hydrophobic layer on an asymmetric hydrophilic polyethersulfone membrane for DCMD studies. Interestingly, this process ended up completely hydrophobizing the other originally hydrophilic back surface into a hydrophobic one as well. Evkens et al. [26] explored a variety of coating techniques including vacuum plasma technology and atmospheric plasma technique on commercially available flat polyethersulfone membrane (MicroPES 2F) to develop efficient hydrophobic-hydrophilic structures for successful DCMD. Nonsolvent thermally induced phase separation (NTIPS) method was used to fabricate a novel dual-layer membrane [27]. It had a thin hydrophobic PVDF top-layer and a relatively thick hydrophilic PVDF-polyvinyl alcohol sub-layer to achieve high flux in DCMD. Strategies other than such composite structures are being pursued to enhance MD flux such as breaking the hydrogen bonds in water via gold nanoparticlesadsorbed ceramic rods (AuNPs@CRs) and enhancing the water vapor pressure (Chen et al., 2018 [28]).

We have been employing porous coatings of fluorosiloxane deposited on porous hydrophobic polypropylene hollow fiber surfaces by plasma polymerization for quite some time [2,15–18]. The coatings were highly porous and applied for a very short time to develop near superhydrophobicity [16] without affecting the water vapor flux much via reduction of surface pore size and porosity. Since we have already studied and modeled DCMD behavior of large hollow fiber modules where the hollow fiber surfaces were modified in the fashion stated above, we have explored here application of this vacuum-based plasma polymerization technique on flat hydrophilic PVDF membranes commercially available for studying DCMD performances.

The plasma polymerization time was systematically varied over a 10x time period to find out how the contact angle, LEP, bubble point and the maximum pore diameter of the membrane varied. The desalination performance of each coated membrane was studied in DCMD for a particular feed salt concentration level and a variety of temperature differences. For a few coated systems, a seawater-level higher salt concentration and much lower ΔT values were also used.

Potentially one can have three types of structures of a hydrophobichydrophilic membrane: integral composites; stacked composites; laminated composites. The surface of a hydrophilic membrane can be

modified in a variety of ways as we have done here and elsewhere by plasma polymerization [26] as well as by surface modifying macromolecules [9] or dual layer NTIPS [27]. We may call these integral composites. A second method involves stacking a flat hydrophobic porous membrane over a flat hydrophilic porous membrane and developing a stacked composite structure. In this study, we also investigated this second method. Therein the performances of a stacked composite of a thin porous hydrophobic ePTFE membrane supported by a hydrophilic PVDF porous membrane substrate employed earlier in the preparation of coated membranes were compared with the performances of the thin hydrophobic ePTFE membrane only without the porous hydrophilic PVDF membrane at the bottom. A third method involves preparing a laminated composite of one membrane over another appropriately sealed or joined together. An example is provided in Ref. [29] where two hydrophobic PTFE sheets were joined together. This structure was not studied here.

2. Experimental

2.1. Materials and chemicals

Porous hydrophilic membranes of PVDF were obtained from MilliporeSigma, Bedford, MA and Pall Corp, Port Washington NY. The relevant properties of these two membranes are listed in Table 1. These membranes were used as substrates for plasma coating. A highly porous hydrophobic fluorosiloxane coating was deposited on the surface of the substrate membrane by vacuum-based plasma polymerization (Applied Membrane Technology Inc., Minnetonka, MN).

Five different plasma polymerization times were used (see Table 2). Designation AKS-6591 involved the lowest plasma exposure;

Table 1Properties of base hydrophilic PVDF membranes.

Base hydrophilic membranes of PVDF	d _m (μm) Mean pore size	ε _m (%) Porosity	δ_{m} (µm) Membrane thickness
MilliporeSigma (HVLP)	0.45	70	125
Pall	0.1	82	78.2

Table 2
List of surface modified membranes.

 $Plasma\ polymerized\ hydrophobic\ coating\ on\ hydrophilic\ membrane$

AKS-6591-1-Millipore AKS-6591-2-Millipore AKS-6591-1-Pall

AKS-6591-2-Pall

AKS-6592-1-Millipore

AKS-6592-2-Millipore AKS-6592-1-Pall AKS-6592-2-Pall

AKS-6593-1-Millipore AKS-6593-2-Millipores AKS-6593-1-Pall AKS-6593-2-Pall

AKS-6594-1-Millipore AKS-6594-2-Millipore AKS-6594-1-Pall AKS-6594-2-Pall

AKS-6595-1-Millipore AKS-6595-2-Millipore AKS-6595-1-Pall AKS-6595-2-Pall

Table 3 List of various stacked phobic-philic composite membranes

Composite membranes

ePTFE M-020B (30 μm thick 0.2 μm pore size) (top) 0.1 μm pore size Pall hydrophilic membrane

ePTFE M-010 (85 μm thick 0.1 μm pore size) (top) 0.1 μm pore size Pall hydrophilic membrane

ePTFE M-020A (70 μm thick 0.2 μm pore size) (top) 1.1 μm pore size Pall hydrophilic membrane

designation AKS-6595 involved the highest plasma exposure. The time intervals employed were 1X, 2X, 3X, 6X and 10X. Suffix-1 and Suffix-2 indicate the position of the membrane substrates in the reactor for each set. Since the properties of plasma polymers vary with the position of

to vaporization of water from the hot brine feed solution through membrane pores would get this liquid level controller to activate a pump to take in fresh deionized (DI) water from a makeup water storage tank. The hot brine flow rate was varied between 300 and 750 ml/ min. The distillate flow rate was varied between 490 and 900 ml/min.

Platinum RTD sensors (Model RTD-NPT-72-E-1/4-HH804-CONN, Omega, Stamford, CT; Accuracy:0.15 + 0.002T(°C)) connected to digital thermometers (Dual Input Pt100 Platinum RTD meter, Model HH 804, Omega, Stamford, CT; Accuracy: ± 0.05% + 0.2 °C) were employed to measure the inlet and outlet temperatures of the brine as well as the distillate streams through the CPVC cell. Before starting the measurement of the water vapor flux in membrane distillation, the flow rates of the brine out and the distillate out streams were measured manually. The distillate production rate was obtained by the overflow rate from the distillate tank by a weighing machine:

$$N_{\nu}\left(\frac{kg}{m^{2}, h}\right) = \frac{\text{Increase in weight of water}\left(=\text{volume of water transferred(L)} * \textit{waterdensity}\left(\frac{kg}{L}\right)\right)}{\text{membrane area}(m^{2} * \textit{time}(h))}$$
(1)

the substrate with regard to the electrode position in the reactor, position designated -2 is likely to produce more cross-linked coatings as is revealed by the darker color of the coating. The list of these membranes is provided in Table 2. Two samples were prepared under each condition.

In addition, experiments were also done with a stack of two membranes, one on top of the other (Table 3). The bottom membrane was a 0.1 µm pore size Pall hydrophilic PVDF membrane identified in Table 1. The top membrane was hydrophobic and was selected from one of the following three membranes: ePTFE M-020B; ePTFE M-020A; ePTFE M-010 (W L. Gore, Elkton, MD). Table 4 identifies a different type of composite: hydrophobic over a hydrophobic membrane: hydrophobic membrane (PVDF HVHP04700, MilliporeSigma) placed over the same hydrophobic membrane resulting in a phobic-phobic stacked composite.

2.2. Methods and procedures

The DCMD experimental setup (Fig. 1) has been described earlier in Refs. [1,17,18]. The CPVC-based rectangular cell built for and described in Ref. [1] with a membrane area of 0.0011 m² was used here. The differences between the setup in Ref. [1] and here lies in the use of a different constant temperature bath, a water based heating bath (Haake C10, Thermo Electron Corporation, NJ) used to heat the titanium vessel acting as the brine reservoir. The brine used was 1% NaCl solution unless otherwise mentioned; later 3% NaCl solution was also used. In most experiments, the incoming hot brine temperature was varied between 60 °C and 85 °C. The distillate-in temperature was generally around 20 °C. In a few experiments with lower overall temperature differences between the hot brine and the cold distillate, the distillate-in temperature was raised to 35 °C while the hot brine-in temperature was reduced to 45 or 50 °C. A liquid level controller (Warrick Series 16, Gems Sensors & Controls, Plainville, CT) immersed into the brine tank was employed to maintain constant brine concentration in the following fashion. Any lowering of the brine level due

Table 4

125 µm thick (bottom) (Millipore EMD)

PVDF HVHP04700 hydrophobic membrane, 0.1 µm pore size, 0.70 porosity and 125 µm thick (top) (Millipore EMD) PVDF HVHP04700 hydrophobic membrane, 0.1 µm pore size, 0.70 porosity and

Description of stacked phobic-phobic composite membrane.

To check for any salt leakage to the distillate side, the distillate side conductivity was measured using a conductivity meter (Orion 115A+, Thermo Fisher Scientific, Waltham, MA). Any experiment under given conditions was run for around 3 h after steady state was reached. The effective membrane area in the CPVC cell was 11 cm². The membrane in the cell was supported by two PTFE meshes (Part No. ET8800, Industrial Netting, Minneapolis, MN; Part No. 1100T41, McMaster-Carr, Robbinsville, NJ). All experiments were repeated twice.

The porosity of the hydrophilic Pall membrane was determined in the following way [30]. From the large membrane supply, 47 mm diameter (d) membrane samples were cut out. The weight (m) of eight such membranes stacked on top of one other was determined in a balance (Cole-Parmer, Vernon Hills, IL); the thickness (t) of this stack was determined by a caliper (Model No. CD-6" CSX, Mitutoyo, Japan). For a base PVDF polymer density of 1.78 g/cm³ defined as ρ_{base material}, we obtain the membrane porosity ε_m from equations (2a) and (2b):

$$\rho_{\text{sample}} = m/((\pi/4)d^2t)$$
 (2a)

$$\varepsilon_{\rm m} = \left(1 - \frac{\rho_{\rm sample}}{\rho_{\rm base\ material}}\right) x\ 100\% \tag{2b}$$

Contact angle of a water drop on a flat membrane surface was determined by optical tensiometry (Model No. A 100, Rame-Hart Inc., Succasunna, NJ). An amount of liquid ($\sim 10\,\mu L$) was dropped on the membrane sample surface. The liquid drop was adjusted so that it was clearly observed in the eye lens. The liquid entry pressure (LEP) was measured in a flat stainless steel cell (diameter 47 mm; membrane area 13.8 cm²; part # XX4404700, MilliporeSigma, Billerica, MA) in an apparatus described in [31,32]. Both sides of the flat integral composite membrane were tested for the LEP value. Deionized (DI) water was used as the test liquid. A N2 gas cylinder was used to pressurize the water in the cell onto the membrane. The pressure was slowly increased by 1 psig (6.89 kPag) every 2 min. The time gap was required for the pressure to stabilize. The pressure at which drops of water break through continuously was determined to be the LEP. To measure bubble point pressure, the membrane sample of 47 mm diameter was wetted by isopropyl alcohol after which it was put in a bubble point measuring test cell and gas pressure applied [1]. The pressure at which a stream of bubbles was observed downstream of a wetted membrane under gas pressure was designated the bubble point pressure, PBP. The accuracy of the pressure gage was \pm 689 Pa (0.1 psi).

LEO 1530 VP field emission scanning electron microscope (SEM)

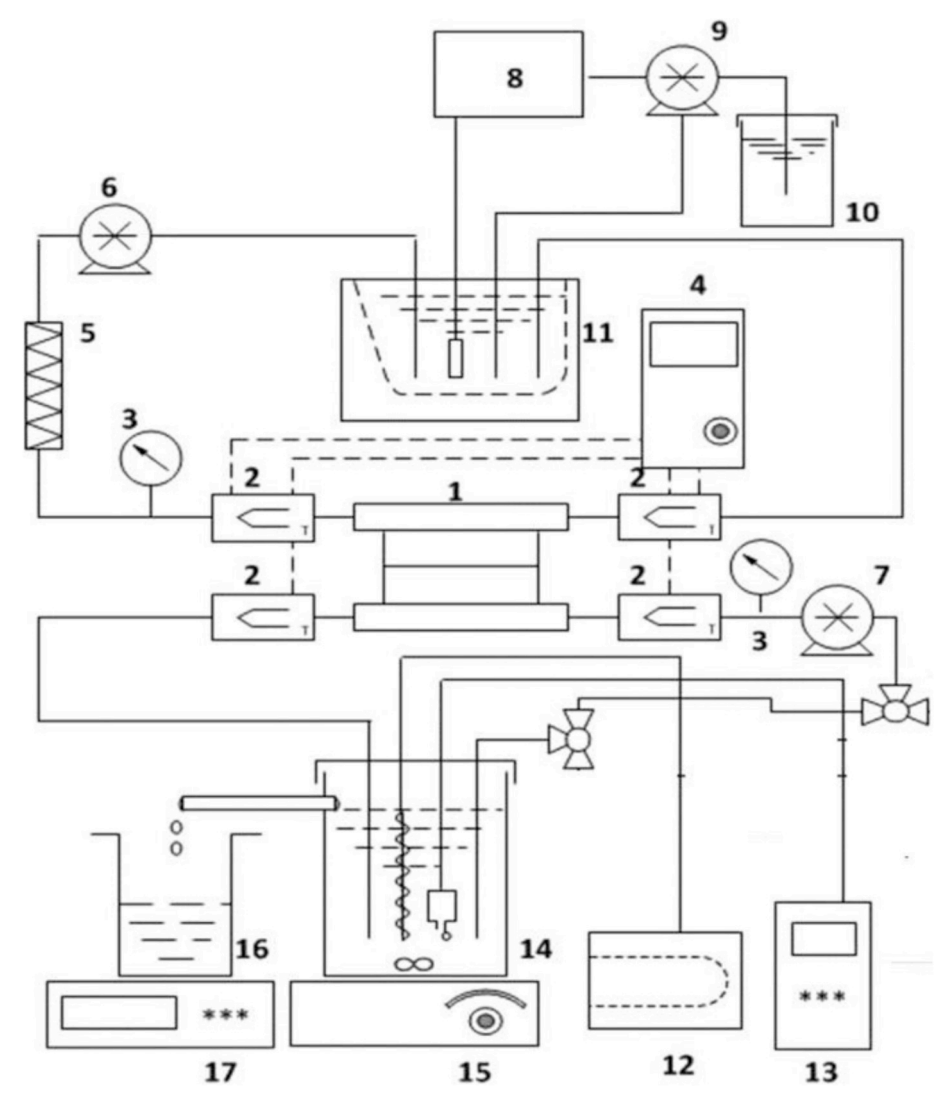


Fig. 1. A schematic of the DCMD setup. 1. Membrane test cell; 2.Thermocouple; 3. Pressure indicator; 4. Digital thermometer; 5. Pre-filter; 6. Brine pump; 7. Distillate pump; 8. Liquid level controller; 9. Make-up pump; 10. Make-up water reservoir; 11. Brine water bath; 12. Chiller; 13. Conductivity meter; 14. Distillate beaker; 15. Magnetic stirrer; 16. Distillate overflow beaker; 17. Weighing balance.

(Carl Zeiss Inc., Peabody, MA) was used to study the cross-section of the plasma-coated region. JSM 7900F Field Emission SEM (JEOL USA,Peabody, MA) was used for the surfaces of the plasma polymerized coated membrane and the substrate membrane. To determine the elements in the plasma-coated region, energy-dispersive X-ray spectroscopy (EDS) was also used for a few samples. The AFM used was Bruker Dimension Icon with ScanAsyst (Bruker, Billerica, MA).

3. Results and discussion

The order of result presentation will be plasma-coated integral composite hydrophobic-hydrophilic membranes followed by stacked hydrophobic-hydrophilic composite membranes. At the end, we deliberate on laminated composites. For the plasma-coated integral composite hydrophobic-hydrophilic membranes, we will first present the results of our measurements of contact angles and LEP values of the complete set of flat plasma-coated membranes. The list includes membranes prepared on both hydrophilic substrates, membranes at two locations in the reactor, namely locations -1 and -2, and five sets of plasma polymerization conditions. Then we will illustrate the detailed membrane distillation behavior of water vapor flux for two sets of membranes exposed to the plasma for different extents of time. Next, we will provide a graphical illustration of the water flux behavior of

almost all of the membranes as a function of the plasma exposure time. SEM micrographs of the coated membrane cross-section and the coated membrane surface will be provided for selected coated membranes followed by EDS plots to identify the presence of different materials in the coating and the substrate. The membrane distillation behavior of the stacked composite membranes of two different types will be illustrated next along with the AFM micrographs of the surfaces of the individual membranes used in particular type of integral or stacked membrane composites.

3.1. Integral composites developed by plasma polymerization

Table 5 lists all plasma-coated membranes of this study. Fig. 2 provides a conceptual background about the effect of plasma polymerization time on the pore mouth dimensions. The process of plasma polymerization under vacuum involves evaporation of appropriate monomers from reservoirs and their interaction with functional groups activated on the substrate polymer surface by the plasma to form ultimately a growing polymer. The growth of this polymer at every pore mouth slowly reduces the open pore dimension as shown in Fig. 2. This also explains why even though the underlying substrate is hydrophilic, water pressure from the hydrophilic side also shows a LEP. Further, we can see from Table 5 that in general, as the time for plasma

Table 5Values of LEP and contact angles of two types of porous hydrophilic membranes having different extents of plasma polymerized porous hydrophobic coating on one surface.

Coated membrane sample	Hydrophilic PVDF substrate		Contact angle in degree		LEP in psig (kPag)	
designation	d _m (μm)	δ_{m} (μm)	Coated	Uncoated	Coated	Uncoated
AKS-6591-1 M*	0.45	125	107	62	9 (62.0)	6 (41.3)
AKS-6591-2 M*	0.45	125	110	54	16 (110.3)	12 (82.7)
AKS-6591-1 P*	0.1	78.2	109	45	17 (117.2)	16 (110.3)
AKS-6591-2 P*	0.1	78.2	108	46	22 (151.6)	18 (124.1)
AKS-6592-1 M*	0.45	125	95	60	14 (96.5)	10 (68.9)
AKS-6592-2 M*	0.45	125	98	65	18 (124.1)	15 (103.4)
AKS-6592-1 P*	0.1	78.2	100	55	23 (158.5)	20 (137.8)
AKS-6592-2 P*	0.1	78.2	110	50	31	28
AKS-6593-1 M*	0.45	125	108	79	(213.7)	(193.0) 11
AKS-6593-2 M*	0.45	125	96	86	(103.4)	(75.8) 16
AKS-6593-1 P*	0.1	78.2	95	25	(131.0)	(110.3)
AKS-6593-2 P*	0.1	78.2	100	86	(172.3)	(137.8)
AKS-6594-1 M*	0.45	125	100	79	(227.5)	(179.2) 23
AKS-6594-2 M*	0.45	125	99	81	(131.0) 25	(158.5)
AKS-6594-1 P*	0.1	78.2	98	86	(172.3)	(193.0)
AKS-6594-2 P*	0.1	78.2	-	-	(193.0) -	(213.7) -
AKS-6595-1 M*	0.45	125	120	117	26 (179.2)	34 (234.4)
AKS-6595-2 M*	0.45	125	95	53	44 (303.3)	46 (317.1)
AKS-6595-1 P*	0.1	78.2	95	95	24 (165.4)	24 (165.4)
AKS-6595–2 P*	0.1	78.2	96	113	21 (144.7)	19 (131)

M* & P* represent Millipore and Pall respectively.

polymerization increases, the value of LEP increases significantly since the effective open pore dimension decreases. The LEP value increases from a low value of 6–9 psig (41.3–62 kPag) for the sample AKS-6591-1 M exposed for the lowest time to the plasma to quite a high value of 44–46 psig (303–317 kPag) for the sample AKS-6595-2 M exposed to the highest time of plasma polymerization. Also consistent with the

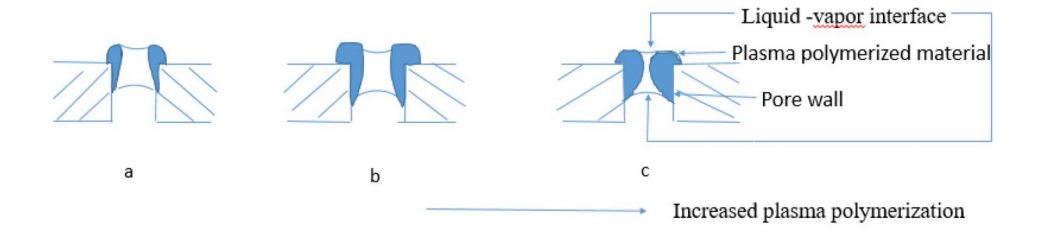
position of the samples with the suffix -2 in the reactor with higher level of plasma polymerization, we see that almost every such sample has a higher LEP than samples with the suffix -1.

The backside of samples beginning with designation AKS-6595 show hydrophobic behavior from contact angle measurements. This has resulted from considerable leakage of plasma to the back side of the membrane making it have many hydrophobic patches. There is a trend in contact angle data in this direction as time for plasma polymerization was increased. Future efforts will take countermeasures to prevent it. For other samples, AKS-6591 to AKS-6594, the backside (namely, the uncoated side) continued to remain hydrophilic even though there is some variation due possibly to very limited intrusion of plasma.

For the series of membranes AKS- – 2 M, water contact angle for the coated side of the membrane varies between 95° and 110°. All of them are hydrophobic and above 90°. The durations of plasma polymerization for different experiments were not long. There will always be variation between locations to locations unless a heavy coating is deposited. On another aspect of the results, AKS-6595–2 P membranes have the smallest LEP value when it has the longest plasma polymerization time. It is known that LEP is a reflection of the largest pore size of the membranes. The commercially available substrate PVDF membranes have a broad pore size distribution. It is likely that the particular membrane had probably somewhat larger pores leading to the lowest LEP.

Fig. 3(a) and (b) illustrate variation of water vapor flux in DCMD with the hot brine temperature and the hot brine flow rate respectively for plasma coated membranes with designations of AKS-6591-1 and AKS-6591-2, both based on the Millipore substrate. Since these two samples have the lowest amount of plasma exposure, one would expect the highest fluxes; in fact the values are quite high. Since reactor location -2 involves higher amount of polymerization, clearly we see a lower flux compared to the sample exposed to reactor location -1. Fig. 3(c) and (d) show similar results for AKS-6591-1 and AKS-6591-2 based on the Pall substrate. However, at the highest flow rate in Fig. 3(c), the two data points appear to overlap each other.

In Fig. 4(a) and (b), essentially a similar water flux behavior is observed for plasma-coated membranes having the designations AKS-6593-1 and AKS-6593-2 (Millipore). However, since the plasma polymerization times for these samples are considerably longer than those of the AKS-6591-1 and AKS-6591-2, the water vapor fluxes are significantly lower. We see a similar water vapor flux behavior in Fig. 4(c) and (d) for the corresponding membranes utilizing the Pall substrate. Higher plasma polymerization time reduces pore opening dimensions leading to a significant reduction in the water vapor flux. There is an added effect. The difference between the observed fluxes from membranes obtained from positions -1 and -2 in the reactor are significantly reduced. In Fig. 4(d), the data points for the highest flow rate are almost overlapping each other. Results of water vapor fluxes from membranes corresponding to AKS-6594-1 and AKS-6594-2 (Millipore) (not shown here) are even closer.



-From figures a, b, c it is clear that the pore size decreases with increase in plasma polymerization time.

-PPtc> PPtb> PPta

Fig. 2. Effect of increased plasma polymerization time (PPt) on the decrease in pore mouth opening dimension.

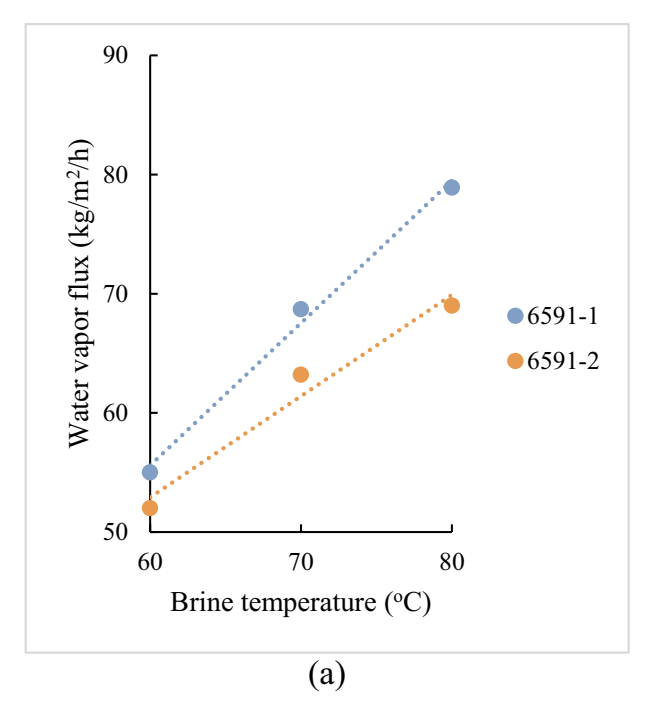


Fig. 3. (a) Water vapor flux values for different brine temperatures at a constant brine flow rate of 490 ml/min and distillate flow rate of 750 ml/min.; (b) water vapor flux values at various brine flow rates and a constant brine inlet temperature of $70\,^{\circ}$ C. Both are for plasma-coated membranes of designations AKS- 6591-1 and AKS-6591-2 (Millipore).

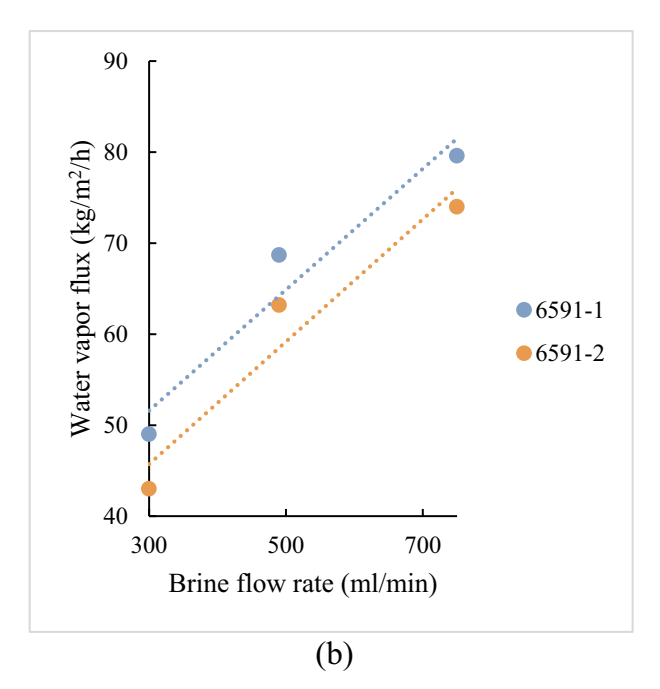


Fig. 3. (continued)

Fig. 5 compares the surface of a hydrophilic PVDF (Pall) membrane before and after plasma polymerization. Figs. 5(a) and (b) show respectively the results of 2D and 3D AFM scans of the hydrophilic PVDF membrane as such. Figs. 5(c) and (d) illustrate respectively the results of 2D and 3D AFM scan of the plasma polymerized surface of PVDF-Pall-AKS-6595-2. From these figures, it appears that plasma polymerization process reduces surface roughness via the coating over an uneven surface. Figs. 5 (a) and (b) clearly show the nature of the surface roughness on top of the porous PVDF membrane. Such surface

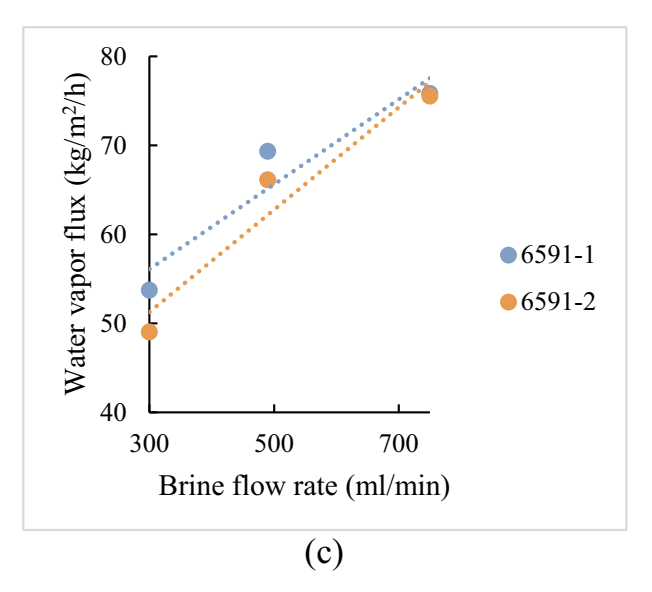


Fig. 3. (c) Water vapor flux values at various brine flow rates and a constant brine inlet temperature of 70 °C; (d) water vapor flux values for different brine temperatures and a constant brine flow rate of 490 ml/min and distillate flow rate of 750 ml/min. Both are for plasma-coated membranes of designations AKS-6591-1 and AKS-6591-2 (Pall).

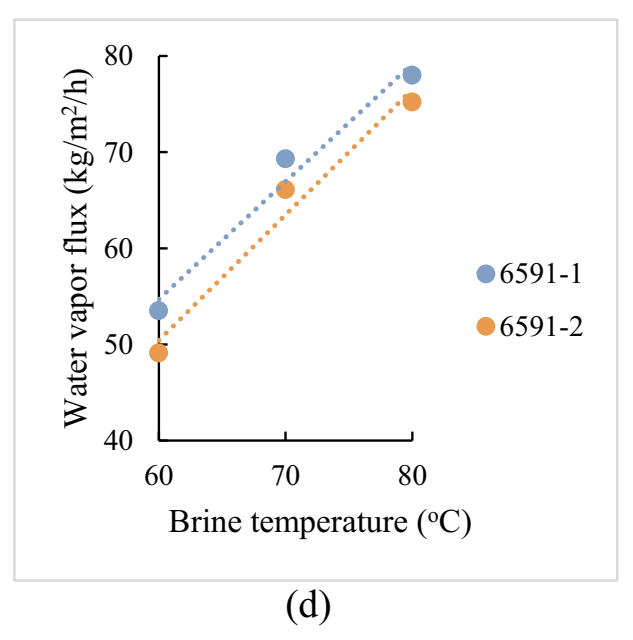


Fig. 3. (continued)

roughness may have other utility as we will see later in this study.

Fig. 6 consolidates the general trend of water vapor flux behavior observed for different plasma polymerization times by plotting the data for four conditions at two reactor locations for two specific hot brine temperatures, other conditions remaining constant; data are provided for both hydrophilic substrates, Millipore (M) and Pall (P). In spite of the scatter, it is clear that water vapor flux decreases with increased polymerization time; also reactor 2 position with more polymerization always yields lower flux. The d_{max} value of the coated membrane via Eq. (3)

$$d_{max} = \frac{4 \gamma \cos\theta}{P_{RP}} \tag{3}$$

(where γ is the surface tension of water, θ is the contact angle and d_{max}

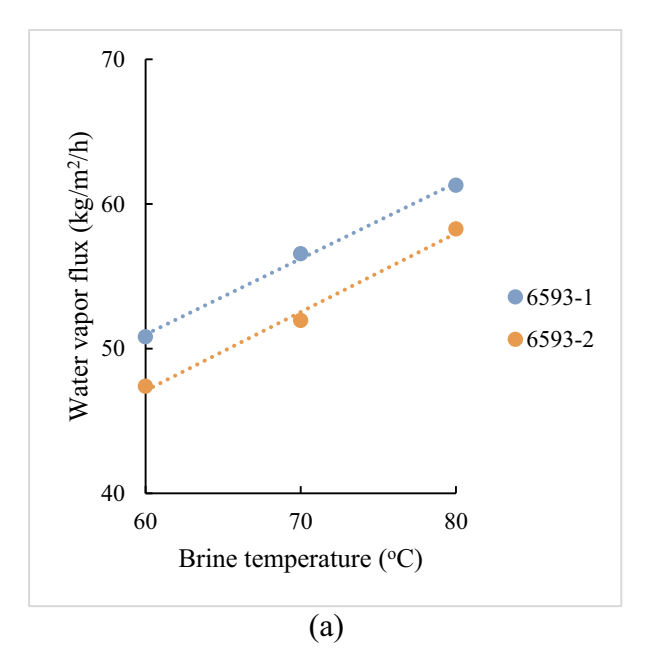


Fig. 4. (a) Water vapor flux values for different brine temperatures and a constant brine flow rate of $490 \, \text{ml/min}$ and distillate flow rate $750 \, \text{ml/min}$; (b) water vapor flux values at various brine flow rates and a constant brine inlet temperature of $70 \, ^{\circ}\text{C}$. Both are for plasma-coated membranes having designations AKS-6593-1 and AKS-6593-2 (Millipore).

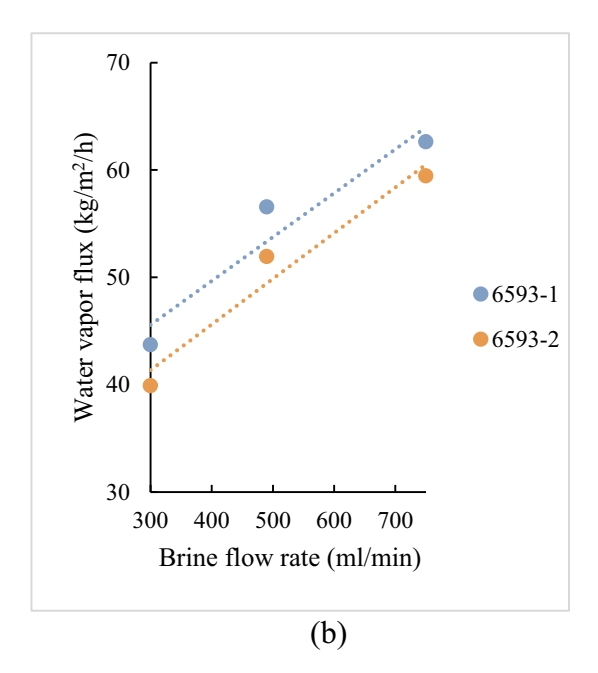


Fig. 4. (continued)

is the largest pore diameter) was also calculated for a few membrane samples (Table 6) from the measured values of the bubble-point pressures P_{BP} (Table 6). Clearly, position 2 in the reactor and higher polymerization time lead to a smaller d_{max} due to a higher extent of coating and corresponding reduction in the pore size (Fig. 2).

Fig. 7(a) provides the SEM micrograph of the cross section of the surface region of the plasma-coated membrane AKS-6593-1 Millipore. It is clear that the plasma had started penetrating the pores in varying degrees at different locations. Fig. 7b (top) illustrates the SEM micrograph of the base Millipore HVLP membrane whereas that of the plasma coated surface of AKS-6593-2 Millipore is shown in the bottom micrograph. One can clearly see how the underlying porous structure of

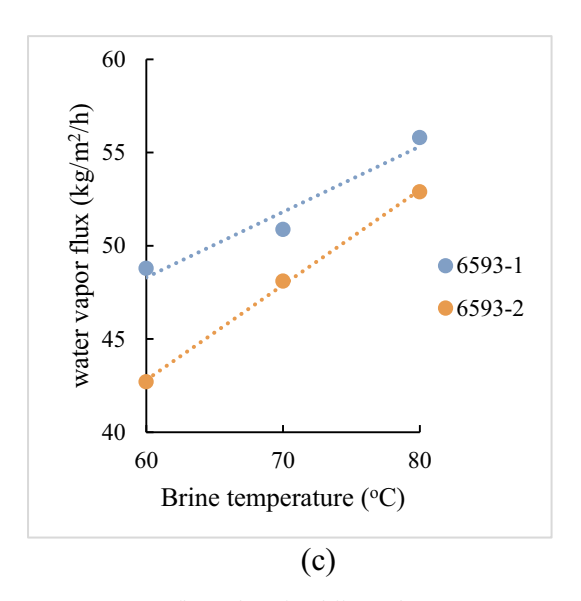


Fig. 4. (c) Water vapor flux values for different brine temperatures and a constant brine flow rate of 490 ml/min and distillate flow rate 750 ml/min; (d) water vapor flux values at various brine flow rates and a constant brine inlet temperature of 70 °C. Both are for plasma-coated membranes, designations AKS-6593-1 and AKS-6593-2 (Pall).

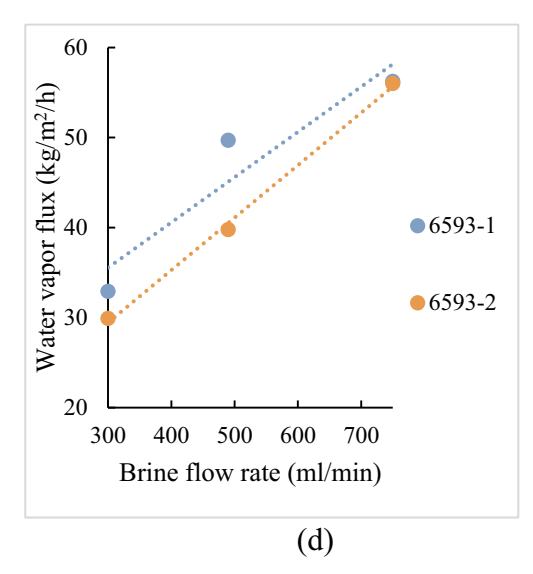


Fig. 4. (continued)

the hydrophilic membrane was being covered up by the plasma polymerized coating.

Fig. 7c and d provide EDS plots of the membrane AKS-6593-1-M at two locations indicating the presence of silicon and fluorine on the surface from the plasma polymerized fluorosiloxane coating. The SEM of the region focused is shown on the left hand side in each figure. The silicon peak is on the low side. Two different monomers, one with silicon and one with fluorine, were used during plasma polymerization. There is no fixed structure of the fluorosiloxane polymer as such since as time progresses the composition varies due to the short time used for polymerization.

3.2. Stacked hydrophobic-hydrophilic composite membranes

The DCMD results from the configuration where a flat hydrophobic membrane facing the hot brine is backed up by a flat hydrophilic membrane whose other surface is exposed to the cold distillate stream will be illustrated now. This configuration can be easily achieved in

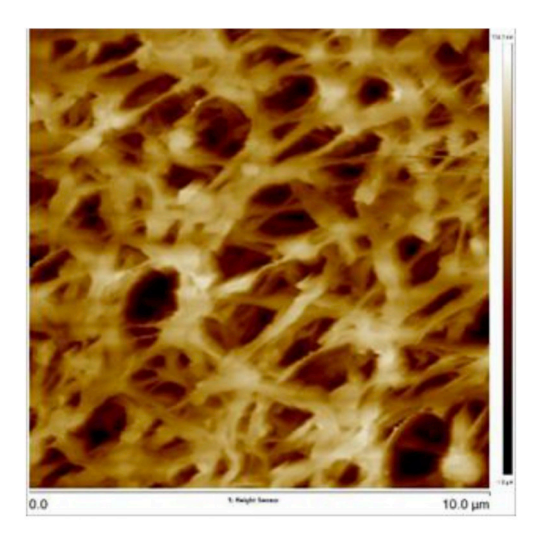


Fig. 5. (a), (b). AFM images of PVDF (Pall) membrane: (a) and (b) show AFM 2D and 3D images respectively at a scan range of $10\mu m$ (surface roughness is 205 nm).

(a)

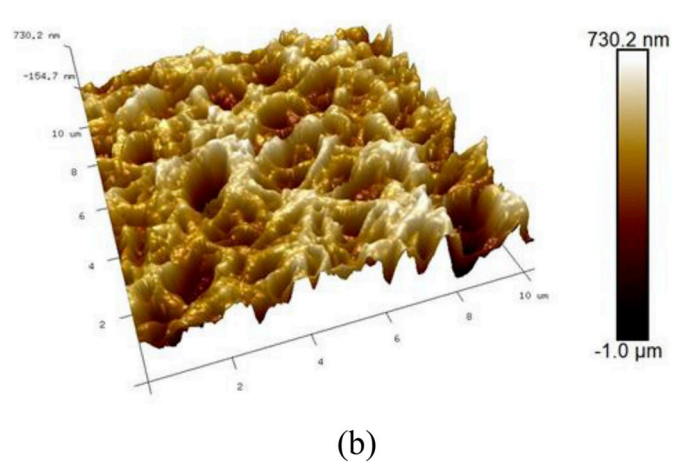


Fig. 5. (continued)

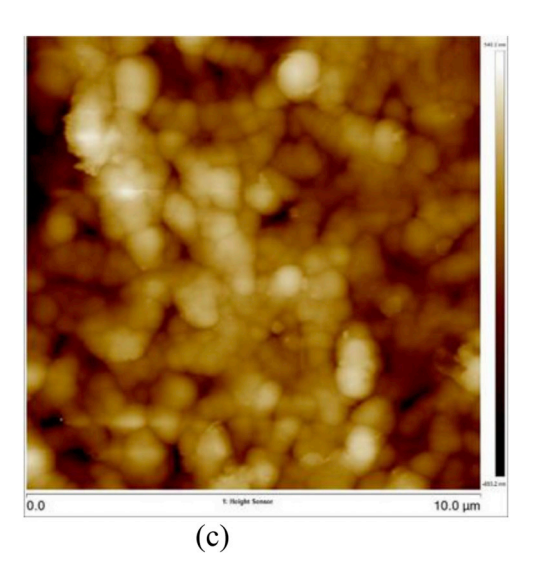


Fig. 5. (c), (d). AFM images of PVDF-Pall-AKS-6595-2: (c) and (d) show respectively AFM 2D and 3D images at a scan range of 10 μ m (surface roughness is 129 nm).

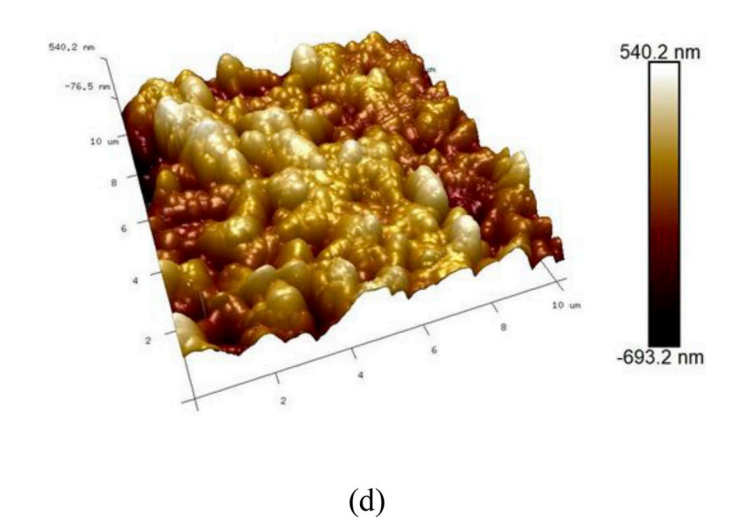


Fig. 5. (continued)

 $\label{eq:constraints} \textbf{Table 6} \\ \text{LEP and bubble point pressures and corresponding } d_{max} \text{ values for a few samples.}$

red membrane sample LEP in psig gnation (kPag)		d _{max} (μm)	Bubble point pressure	
Coated	Uncoated		psig (kPag)	
15	11	2.8	8.8(60.6)	
(103.4)	(75.8)			
19	16	2.2	8.8(60.6)	
(131.0)	(110.3)			
25	20	1.6	16.2(111.6)	
(172.3)	(137.8)			
33	26	1.2	16.6(111.6)	
(227.5)	(179.2)			
19	23	2.2	8.8(60.6)	
(131.0)	(158.5)			
25	28	1.6	8.8(60.6)	
(172.3)	(193.0)			
26	34	1.6	8.8(60.6)	
(179.2)	(234.4)			
	(kPag) Coated 15 (103.4) 19 (131.0) 25 (172.3) 33 (227.5) 19 (131.0) 25 (172.3) 26	(kPag) Coated Uncoated 15 11 (103.4) (75.8) 19 16 (131.0) (110.3) 25 20 (172.3) (137.8) 33 26 (227.5) (179.2) 19 23 (131.0) (158.5) 25 28 (172.3) (193.0) 26 34	(kPag) (µm) Coated Uncoated 15 11 2.8 (103.4) (75.8) 19 16 2.2 (131.0) (110.3) 25 20 1.6 (172.3) (137.8) 33 26 1.2 (227.5) (279.2) 19 23 2.2 (131.0) (158.5) 25 28 1.6 (172.3) (193.0) 26 34 1.6	

M* & P* represent Millipore and Pall respectively.

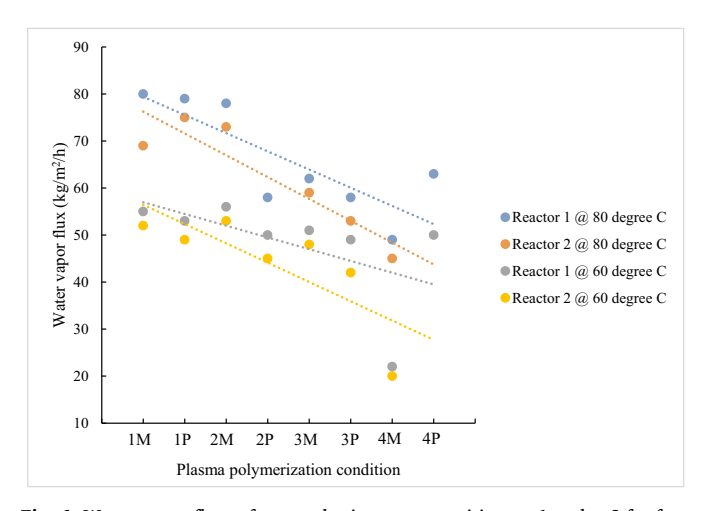


Fig. 6. Water vapor fluxes for samples in reactor positions -1 and -2 for four plasma polymerization times AKS-6591, AKS-6592, AKS-6593 and AKS-6594 (corresponding to 1x, 2x, 3x and 6x times that for AKS-6591) and two brine temperatures, $80\,^{\circ}$ C and $60\,^{\circ}$ C (brine flow rate 490 ml/min, distillate flow rate 750 ml/min). Substrate designations: Millipore-M; Pall-P.

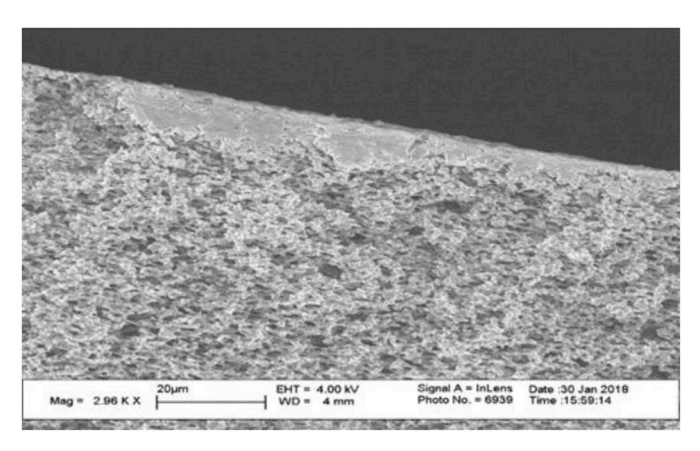
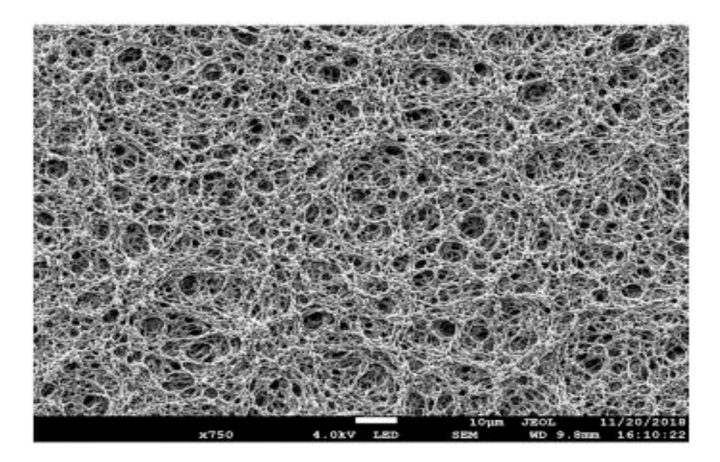


Fig. 7a. Cross sectional SEM image of AKS-6593-1 Millipore with 10 nm gold coating.



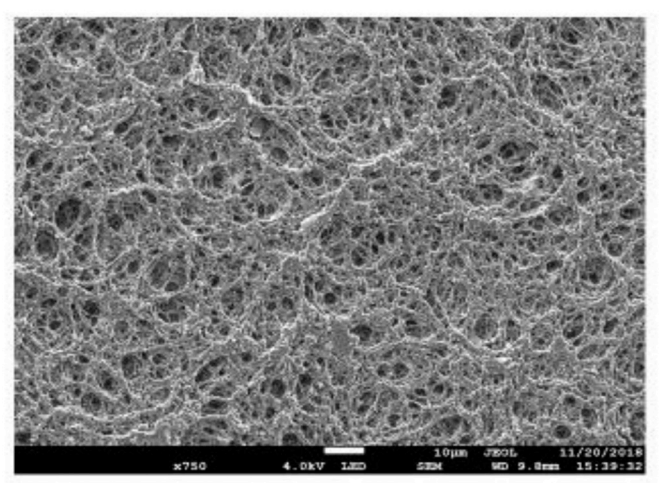


Fig. 7b. Surface SEM image of virgin Millipore HVLP membrane with $12\,\mathrm{nm}$ carbon coating (top) and that of AKS-6593-2 Millipore with $12\,\mathrm{nm}$ carbon coating (bottom).

practice. Fig. 8a and b illustrate results for the ePTFE membrane M020B (30 μ m thick, 0.2 μ m pore size) backed up by a Pall hydrophilic 0.1 μ m pore size membrane. The figures also provide results for the ePTFE membrane without the porous hydrophilic membrane below it. It is very clear that the water vapor flux for a single ePTFE membrane is less than that of the corresponding composite membrane by an average of 25–30 kg/m²-h. The thesis by Puranik [32] provides additional data for this system. Those data essentially reproduce the observed single ePTFE M020B membrane flux behavior obtained earlier by Li and Sirkar

[1]. We see a similar behavior (Fig. 9a and b) for the observed flux when a different ePTFE membrane M020A ($70\,\mu m$ thick $0.2\,\mu m$ pore size) is backed up by the same Pall hydrophilic $0.1\,\mu m$ pore size membrane. The stacked hydrophobic-hydrophilic flat composite membrane however, dramatically outperforms the single hydrophobic membrane.

What could contribute to such a behavior of the observed water vapor flux? We postulate the following. When the backside of a single ePTFE membrane is exposed to the flowing cold distillate stream, the cold water encounters two kinds of surface depressions on the backside of the ePTFE membrane, one due to any pore mouth and another due to any surface roughness elements. The mild above atmospheric pressure in the flowing cold distillate easily overcomes any surface roughness elements when the backside of the hydrophobic polymer surface has flowing distilled water everywhere (without of course penetrating the pores of the hydrophobic membrane). On the other hand, when there is a porous hydrophilic stacked backing membrane on the backside of an ePTFE membrane, there is no such possibility of overcoming the small surface depressions at the backside of the hydrophobic ePTFE membrane unless the distillate side liquid pressure is significantly higher.

Hence, there is a very thin air gap at every surface depression which reduces the conductive heat loss from the hydrophobic ePTFE membrane at the top, generating a significantly higher flux. In effect there is potentially a superhydrophobic type of behavior due to surface roughness at the backside of the ePTFE membrane which allows very thin layers of air to be trapped. We have observed an identical behavior [32] (not shown here) when another ePTFE membrane M010 (85 µm thick 0.1 µm pore size) is backed up by the same Pall hydrophilic membrane vis-à-vis a bare ePTFE M010 membrane. Such possibilities of potential superhydrophobicity presumes that the hydraulic pressure at that location is less than the LEP needed to overcome the dimensions of the surface depressions. This also suggests that the conventional practice in large module development of providing a MD membrane support via a very coarse hydrophobic mesh below a hydrophobic membrane with a fine pore size may not be the best strategy in terms of flux enhancement

The AFM scans of the surface of an ePTFE membrane (Fig. 10) clearly shows the surface roughness elements due to the pores as well as other local roughness elements. Although Fig. 10 is for ePTFE M020B, similar figures are also available for other membranes. Such roughness elements are also clearly visible in Fig. 5(b) of the Pall membrane except they belong to a hydrophilized surface. It is useful to mention that wetting prevention of the feed membrane surface in membrane distillation through superhydrophobicity and recharging an air layer on the membrane surface has been found to be useful in reducing the ill effect of surfactants [33].

Such air gaps facilitate achieving higher flux by reducing conductive heat loss across the membrane thickness. This leads to an increase in feed brine temperature and therefore its vapor pressure and the subsequent water vapor flux. We demonstrate this type of effect also by studying the performance of a stacked hydrophobic-hydrophobic membrane using a PVDF HVHP04700 hydrophobic membrane (0.1 μm pore size, MilliporeSigma) over an identical membrane. Fig. 11 illustrates this behavior. The brine inlet temperature was varied from 65 °C to 80 °C for a brine inlet flow rate 480 mL/min, a distillate inlet flow rate 488 mL/min and distillate inlet temperature 20 °C. At 75 °C, the flux of one hydrophobic PVDF HVHP04700 membrane was 29.1 kg/m²h.whereas the flux of two PVDF HVHP04700 membranes was 17.9 kg/ m²-h, 61.5% of that for a single membrane. At 80 °C, the flux for one membrane was 37.4 kg/m²-h; the flux of two membranes was 23.2 kg/ m²-h, 62.0% of that for a single membrane. These results suggest the possibility of a thin air gap between the two membranes; it reduces conductive heat flux, resulting in less than 50% flux reduction in spite of increasing the membrane thickness by a factor of two.

The much higher water vapor flux values obtained in this study with composite hydrophobic ePTFE membranes supported by a porous hydrophilic PVDF membrane have been compared in Fig. 12 also with the

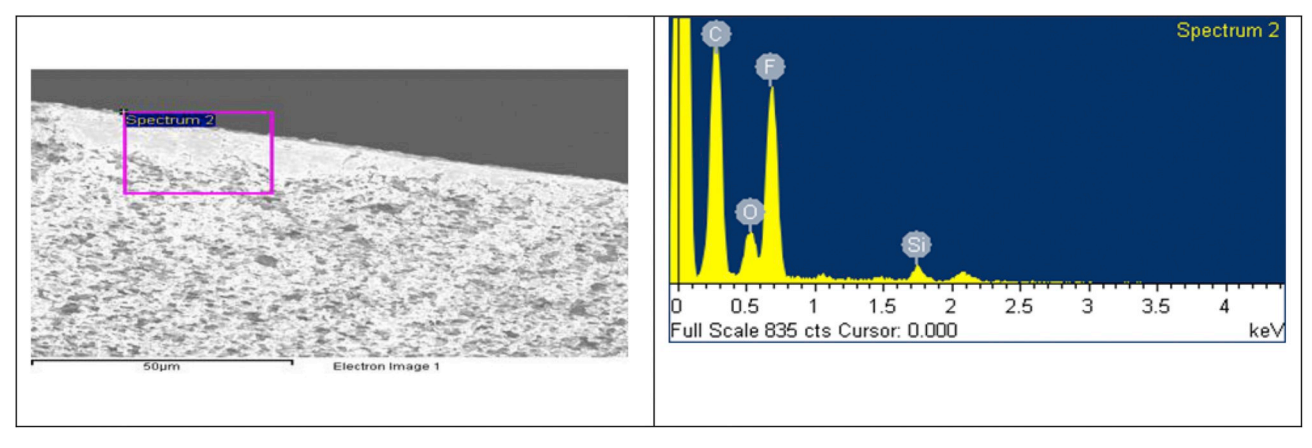


Fig. 7c. Surface EDX image of one location of the AKS-6593-1 Millipore with 10 nm gold coating with the cross section image on the left side.

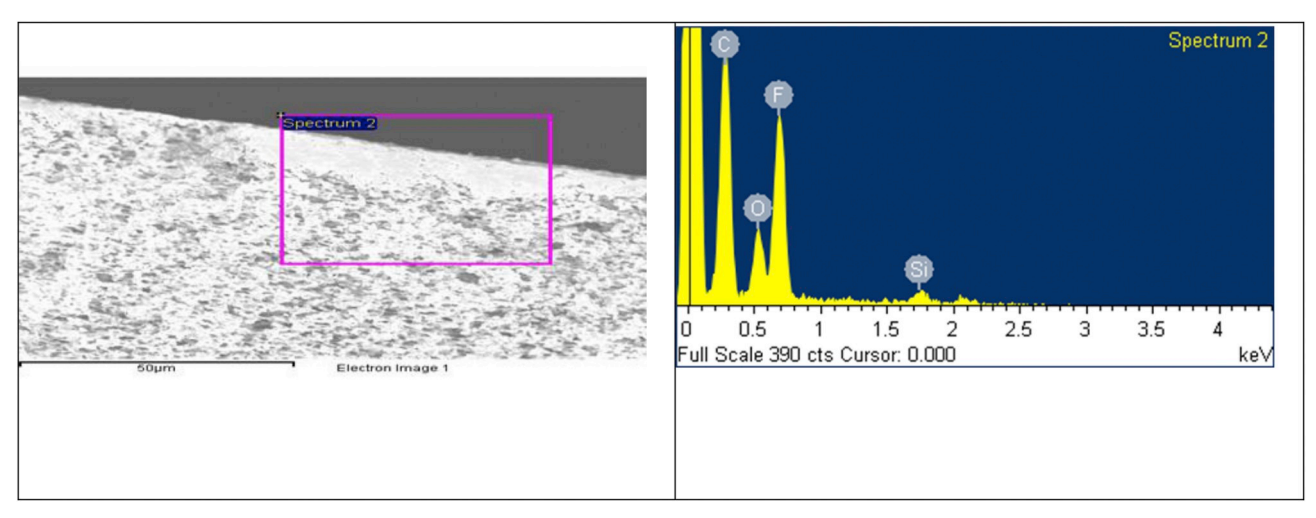


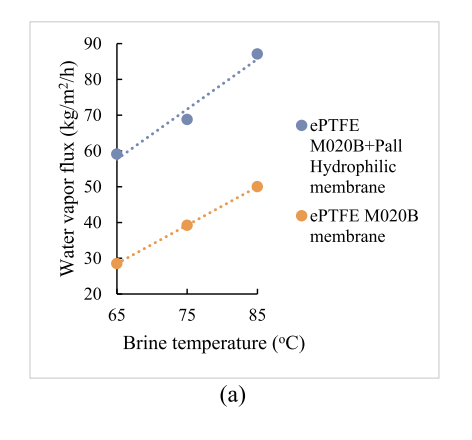
Fig. 7d. Surface EDX image of AKS-6593-1 Millipore with 10 nm gold coating with the cross section image on the left side from a location different from that of Fig. 7c.

data from single hydrophobic ePTFE membranes gathered in the same test cell in Ref. [1] for brine entering at 65 °C. The brine flow rates in the cell were identical for both sets of data. The distillate flow rates used in this work are a bit higher. However, the effect of this difference is limited since it is well known (see also [1]) that distillate side thermal polarization effects are low especially if its temperature is low. An item of issue with such composite membranes is whether there will be any change in brine feed side turbulence vis-à-vis single membrane. The feed channel dimensions in the test cell are essentially unaffected by the increase in the number of membranes from one to two. It is difficult to

conclude whether there will be any effect on the flow pattern in the feed side boundary layer. Turbulence-induced increase in hydraulic pressure cannot increase vapor pressure of water vapor, which is the ultimate driving force for water vapor transport. On the other hand, it can lead to leakage as we have seen in our VMD studies [31].

3.3. Laminated composite membranes

Chen et al. [29] studied successfully the DCMD behavior of a laminated composite consisting of two porous hydrophobic membranes



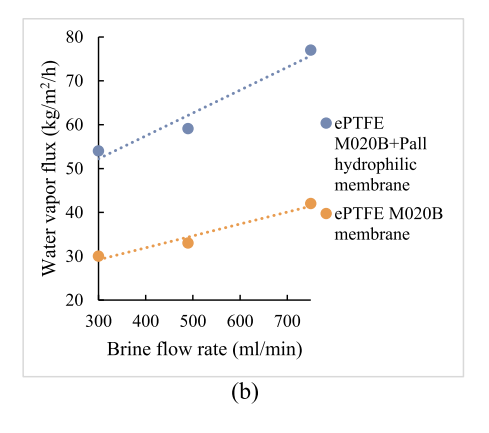
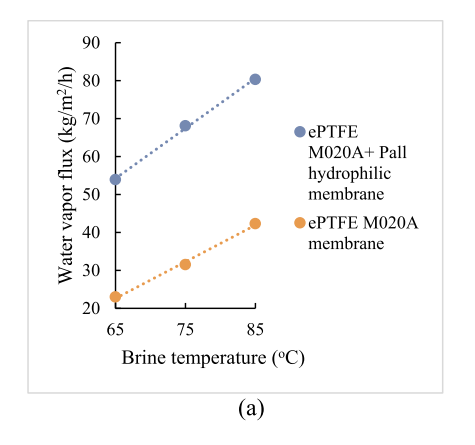


Fig. 8. (a). Water vapor flux values for different brine temperatures and a constant brine flow rate of 490 ml/min and a distillate flow rate of 750 ml/min.; (b). Water vapor flux values at various brine flow rates and a constant brine inlet temperature of 65 °C. The membranes are: ePTFE M020B hydrophobic membrane and a composite of ePTFE M020B hydrophobic membrane backed up by one 0.1 μm Pall hydrophilic membrane.



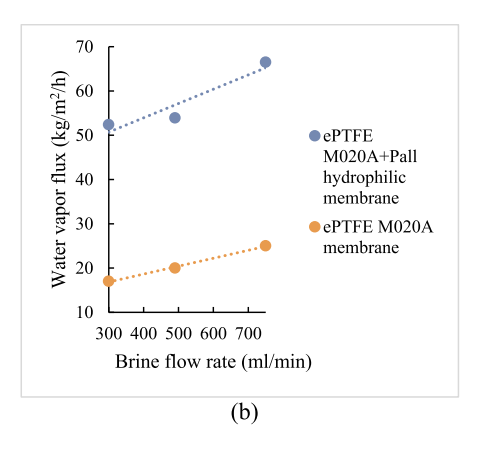


Fig. 9. (a). Water vapor flux values for different brine temperatures and a constant brine flow rate of 490 ml/min and distillate flow rate of 750 ml/min.; (b). Water vapor flux values at various brine flow rates and a constant brine inlet temperature of 65 °C. The membranes are: ePTFE M020A hydrophobic membrane and composite of ePTFE M020A hydrophobic membrane and 0.1 μm Pall hydrophilic membrane.

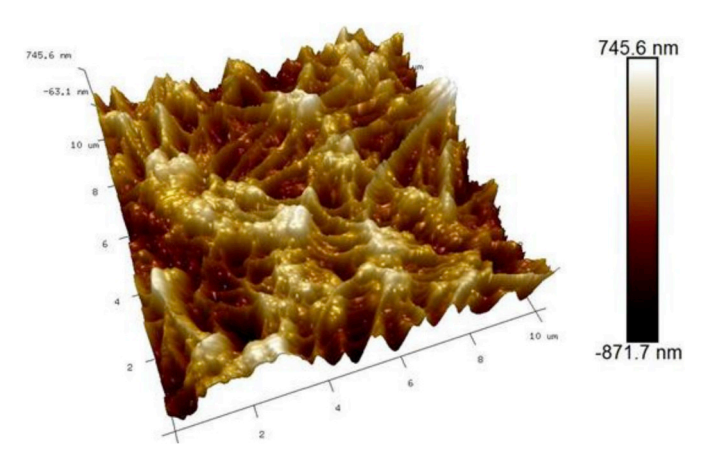


Fig. 10. AFM 3D image of ePTFE M-020B at a scan range of 10 μm (surface roughness is 195 nm).

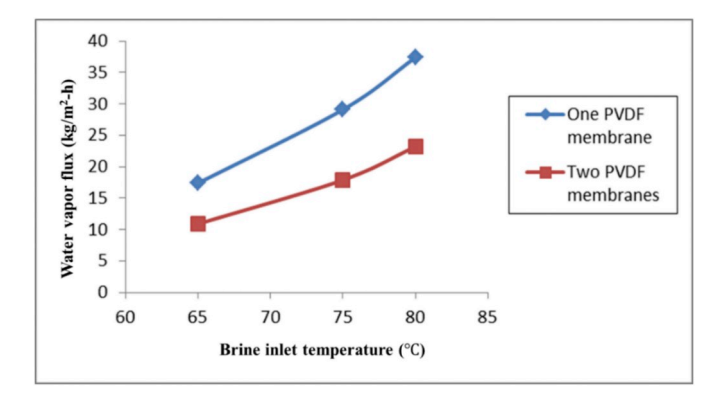


Fig. 11. Experimental results of water vapor flux for one PVDF HVHP04700 membrane and two PVDF HVHP04700 membranes for various brine-inlet temperatures. Brine inlet flow rate, $480\,\mathrm{mL/min}$; distillate inlet flow rate, $488\,\mathrm{mL/min}$; distillate inlet temperature, $20\,^\circ\mathrm{C}$.

joined together. They showed the possibility of bubbles in between the two sheets developing. We did not study any laminated structures here. Much earlier when we were studying DCMD at higher temperatures [34], we had studied a laminated structure of microporous hydrophobic PTFE membranes. We had observed development of bubbles in between the two sheets. Since those experiments were carried out at feed brine temperatures of up to 128 °C and ~ 3 atm, we were afraid of mechanical disruptions and did not pursue it further. The possibility of non-uniform bonding between the two sheets was also of concern. We did not observe any bubble formation here with two membranes stacked on top of each other.

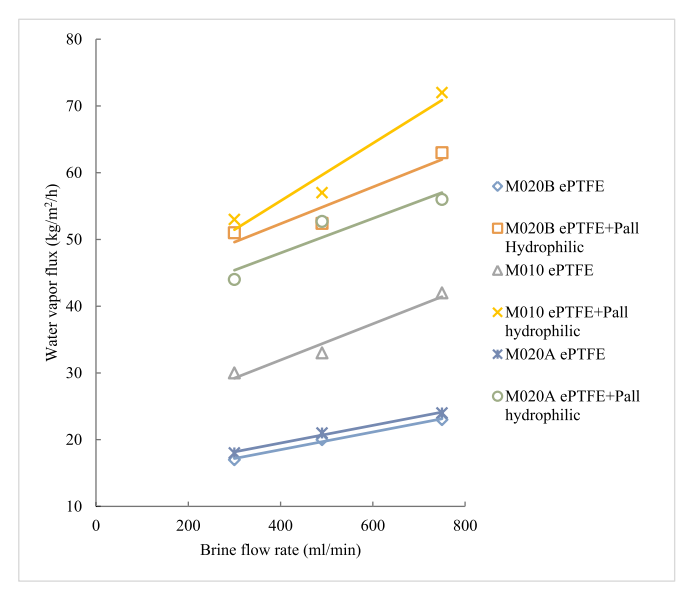
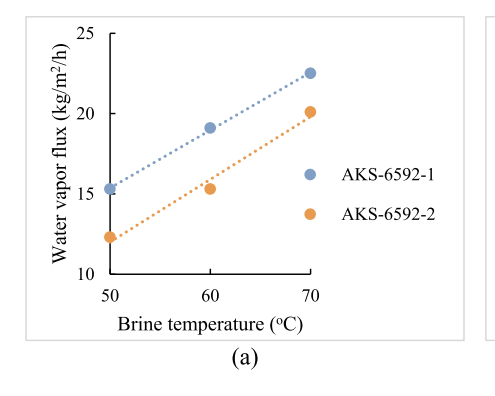


Fig. 12. Comparison of water vapor flux at varying brine flow rates and constant inlet brine temperature of 65 $^{\circ}$ C for single ePTFE membrane from Ref. [1] and composite (ePTFE + Pall hydrophilic) membranes from this work. Distillate flow in at 20 $^{\circ}$ C. Single (ePTFE) membranes are M020B, M010 and M020A (W.L. Gore).

3.4. Behavior of plasma polymerized composite membranes for low $\Delta T\text{-}s$ or higher salt concentration

The water vapor fluxes observed in Figs. 3, 4 and 6 with plasmapolymerized composite membranes are quite high given the small thickness of the air gaps in the hydrophobic part of the composite. In practical energy-efficient DCMD systems, the heat transferred to the distillate stream needs to be recycled so that the value of GOR (gained output ratio) is high (say, at least around 10 kg + of distilled water per kg of steam supplied [2]). To achieve high energy efficiency via recycling of heat gained by the distillate stream, the temperature difference between the hot brine feed and the distillate stream has to be much smaller than what has been used here so far. That will also enhance the thermal efficiency of the DCMD process to as high as $\sim 85\%$ + [2]. To that end, experiments were conducted with lower ΔTs ; the distillate stream entered at 35 °C while the hot brine temperature was varied. Fig. 13(a) and (b) illustrate such results for hydrophilic membranes with a hydrophobic plasma-polymerized coating. The water vapor fluxes are quite high for 50 °C hot brine feed (Fig. 13(a)) resulting in a ΔT of around 15 °C. These enhanced flux values for the very low ΔTs and a feed temperature of only 50 °C are highly encouraging. Further, lower temperature heat sources become amenable to heat extraction by MD.



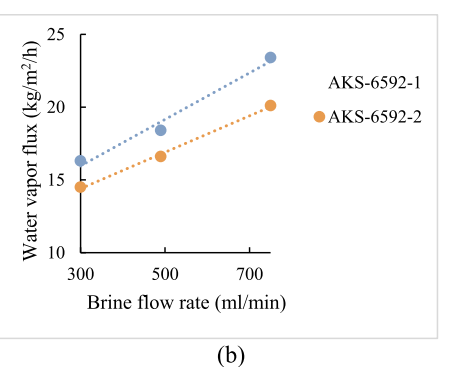


Fig. 13. (a). Water vapor flux values for different brine temperatures and a constant brine flow rate of 490 ml/min and distillate flow rate of 750 ml/min.; (b) Water vapor flux values at various brine flow rates and a constant brine inlet temperature of 60 °C (Distillate temperature, 35 °C)—Membranes used are AKS-6592-1 and AKS-6592-2 Millipore.

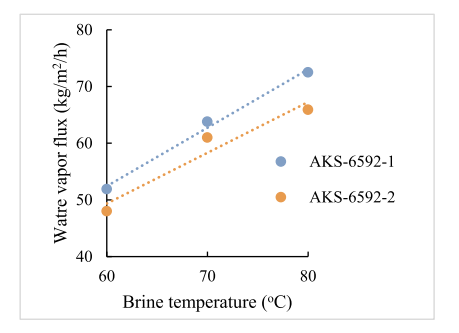


Fig. 14. Water vapor flux values for different temperatures of 3 wt% salt containing brine flowing at 490 ml/min and distillate at 20 °C coming in at 750 ml/min for AKS-6592-1 and AKS-6592-2 Millipore.

All desalination experiments considered so far used 1 wt% salt in feed water. To check whether higher salt concentrations affect the performance significantly, experiments were run with 3 wt% salt in hot brine feed. The results (Fig. 14) show that fluxes are reduced from the corresponding values for 1 wt% brine [32] by around 2–4% for the particular coated hydrophobic-hydrophilic membranes used. This flux reduction level is expected since water vapor pressure driving water vapor flux is reduced by similar amounts due to the corresponding increase in salt concentration.

4. Concluding remarks

A number of techniques have been studied in literature for developing a thin porous hydrophobic coating over a porous hydrophilic substrate for carrying out DCMD-based desalination processes. Vacuum-based plasma polymerization is an effective technique to deposit a thin hydrophobic porous fluorosiloxane coating in a controlled fashion on a thin porous hydrophilic polymeric substrate. Increased polymerization time slowly reduced the opening dimensions of the preexisting pores in the hydrophilic substrate resulting in enhanced values of LEP from both sides of the composite film and reduced water vapor fluxes. Two different locations in the plasma polymerization reactor creating two different times of exposure provide clearly different performances in terms of the LEP and the flux. The measured water vapor fluxes in DCMD are significantly higher than those obtained from conventional hydrophobic membranes under identical fluid mechanical conditions. Correspondingly, one can operate with much lower values of ΔTs and yet achieve reasonable values of water vapor flux. One can also achieve a very high DCMD performance using a stacked composite of a thin porous hydrophobic membrane supported by a porous hydrophilic membrane at the bottom. The flux value is considerably higher than that from the porous hydrophobic membrane only. We postulate the reason for this performance improvement to be as follows. The surface roughness elements of the hydrophobic porous membrane surface facing the hydrophilic membrane at the bottom leads to an air gap in its surface roughness elements and a reduction of conductive heat loss by an insulating air layer. Composite membranes prepared by plasma polymerization methods may also become useful for other types of membrane distillation applications. Specifically, hydrophilic-hydrophobic type of structures with the hydrophilic facing the feed solution containing surfactants etc. [35] would be of interest.

Acknowledgements

Aishwarya Puranik carried out desalination experiments for her MS Thesis at the Otto York Department of Chemical, Biological and Pharmaceutical Engineering, New Jersey Institute of Technology (NJIT). Lydia Rodrigues and John Chau gratefully acknowledge support for this research from the NSF Industry/University Cooperative Research Center for Membrane Science, Engineering and Technology that has been supported via NSF Awards IIP 1034710 and IIP 1822130. We acknowledge W. L. Gore & Associates for providing ePTFE membranes. We acknowledge both MilliporeSigma and Pall Corporation also for providing the PVDF membranes. Lin Li was supported by NJIT during initial planning of the membrane modifications in early 2016 after her research was concluded under a research assistantship from NSF Industry/University Cooperative Research Center for Membrane Science, Engineering and Technology that has been supported via NSF Award IIP 1034710.

References

- L. Li, K.K. Sirkar, Influence of microporous membrane properties on the desalination performance in direct contact membrane distillation, J. Membr. Sci. 513 (2016) 280–293.
- [2] H. Lee, F. He, L. Song, J. Gilron, K.K. Sirkar, Desalination with a cascade of crossflow hollow fiber membrane distillation devices integrated with a heat exchanger, AIChE J. 57 (2011) 1780–1795.
- [3] S. Bandini, C. Costoli, G.C. Sarti, Separation efficiency in vacuum membrane distillation, J. Membr. Sci. 73 (1992) 217–229.
- [4] J.I. Mengual, M. Khayet, M.P. Godino, Heat and mass transfer in vacuum membrane distillation, Int. J. Heat Mass Transf. 47 (2004) 865–875.
- [5] C. Cabassud, D. Wirth, Membrane distillation for water desalination: how to chose an appropriate membrane? Desalination 157 (2003) 307–314.
- [6] J. Mericq, L. Stephanie, C. Cabassud, Vacuum membrane distillation of seawater reverse osmosis brines, Water Res. 44 (2010) 5260–5273.
- [7] T.D. Dao, J.P. Mericq, S. Laborie, C. Cabassud, A new method for permeability measurement of hydrophobic membranes in vacuum membrane distillation process, Water Res. 47 (2013) 2096–2104.
- [8] D.Y. Cheng, S.J. Wiersma, Composite membranes for a membrane distillation system, US Patents, 4,316,772, 1982; 4,419,242 (1983).
- [9] M. Khayet, J. Mengual, T. Matsuura, Porous hydrophobic/hydrophilic composite membranes: Application in desalination using direct contact membrane distillation, J. Membr. Sci. 252 (2005) 101–113.
- [10] M. Khayet, T. Matsuura, J. Mengual, M. Qtaishat, Design of novel direct contact membrane distillation membranes, Desalination 192 (1–3) (2006) 105–111.
- [11] M. Khayet, T. Matsuura, M.R. Qtaishat, J.I. Mengual, Porous hydrophobic/hydrophilic composite membranes preparation and application in DCMD desalination at higher temperatures, Desalination 199 (1–3) (2006) 180–181.
- [12] M. Qtaishat, M. Khayet, T. Matsuura, Guidelines for preparation of higher flux hydrophobic/hydrophilic composite membranes for membrane distillation, J. Membr. Sci. 329 (1) (2009) 193–200.
- [13] M. Su, M.M. Teoh, K.Y. Wang, J. Su, T.-S. Chung, Effect of inner-layer thermal

- conductivity on flux enhancement of dual-layer hollow fiber membranes in direct contact membrane distillation, J. Membr. Sci. 364 (1) (2010) 278–289.
- [14] J.-G. Lee, Y.-D. Kim, W.-S. Kim, L. Francis, G. Amy, N. Ghaffour, Performance modeling of direct contact membrane distillation (DCMD) seawater desalination process using a commercial composite membrane, J. Membr. Sci. 478 (2015) 25 OF
- [15] B. Li, K.K. Sirkar, Novel membrane and device for vacuum membrane distillation-based desalination process, J. Membr. Sci. 257 (2005) 60–75.
- [16] L. Song, Z. Ma, X. Liao, P.B. Kosaraju, J.R. Irish, K.K. Sirkar, Pilot plant studies of novel membranes and devices for direct contact membrane distillation-based distillation, J. Membr. Sci. 323 (2008) 257–270.
- [17] D. Singh, P. Prakash, K.K. Sirkar, Deoiled produced water treatment using direct-contact membrane distillation, I&EC Res. 52 (2013) 13439–13448.
- [18] F. He, J. Gilron, H. Lee, L. Song, K.K. Sirkar, Potential for scaling by sparingly soluble salts in crossflow DCMD, J. Membr. Sci. 311 (2008) 68–80.
- [19] C. Yang, M. Tian, Y. Xie, X.M. Li, B. Zhao, T. He, J. Liu, Effective evaporation of CF₄ plasma modified PVDF membranes in direct contact membrane distillation, J. Membr. Sci. 482 (2015) 25–32.
- [20] Y. Chen, M. Tian, X. Li, Y. Wang, A.K. An, J. Fang, T. He, Anti-wetting behavior of negatively charged superhydrophobic PVDF membranes in direct contact membrane distillation of emulsified wastewaters, J. Membr. Sci. 535 (2017) 230–238.
- [21] L.D. Tijing, Y.C. Woo, W.-G. Shim, T. He, J.-S. Choi, S.-H. Kim, H.K. Shon, Superhydrophobic nanofiber membrane containing carbon nanotubes for highperformance direct contact membrane distillation, J. Membr. Sci. 502 (2016) 158–170.
- [22] E.-J. Lee, A.K. An, T. He, Y.C. Woo, H.K. Shon, Electrospun nanofiber membranes incorporating fluorosilane-coated TiO2 nanocomposite for direct contact membrane distillation, J. Membr. Sci. 520 (2016) 145–154.
- [23] M. Tian, Y. Yin, C. Yang, B. Zhao, J. Song, J. Liu, X.-M. Li, T. He, CF₄ plasma modified highly interconnective porous polysulfone membranes for direct contact membrane distillation (DCMD), Desalination 369 (2015) 105–114.
- [24] S. Jeong, B. Shin, W. Jo, H.Y. Kim, M.W. Moon, S. Lee, Nanostructured PVDF membrane for MD application by an O₂ and CF₄ plasma treatment, Desalination 399 (2016) 178–184.

- [25] X. Wei, B. Zhao, X.M. Li, Z. Wang, B.Q. He, T. He, B. Jiang, CF₄ plasma surface modification of asymmetric hydrophilic polyethersulfone membranes for direct contact membrane distillation, J. Membr. Sci. 407–408 (2012) 164–175.
- [26] L. Eykens, K. De Sitter, C. Dotremont, L. Pinoy, B. Van der Bruggen, Coating techniques for membrane distillation: an experimental assessment, Separ. Purif. Technol. 193 (2018) 38–48.
- [27] Y. Liu, T. Xiao, C. Bao, Y. Fu, X. Yang, Fabrication of novel Janus membrane by nonsolvent thermally induced phase separation (NTIPS) for enhanced performance in membrane distillation, J. Membr. Sci. 563 (2018) 298–308.
- [28] H.-C. Chen, Y.-R. Chen, K.-H. Yang, C.-P. Yang, K.-L. Tung, M.-J. Lee, J.-H. Shih, Y.-C. Liu, Effective reduction of water molecules' interaction for efficient water evaporation in desalination, Desalination 436 (2018) 91–97.
- [29] Y. Chen, R. Zheng, J. Wang, Y. Liu, Y. Wang, X.-M. Li, T. He, Laminated PTFE membranes to enhance the performance in direct contact membrane distillation for high salinity solution, Desalination 424 (2017) 140–148.
- [30] N. Yao, J. Chau, E. Elele, B. Khusid, K.K. Sirkar, D.J. Dehn, Characterization of microporous ECTFE membrane after exposure to different liquid media and radiation, J. Membr. Sci. 532 (2017) 89–104.
- [31] L. Li, K.K. Sirkar, Studies in vacuum membrane distillation with flat membranes, J. Membr. Sci. 523 (2017) 225–234.
- [32] A.A. Puranik, "Effect of Composite Membranes on Direct Contact Membrane Distillation Flux", MS Thesis, Chemical, Biological and Pharmaceutical Engineering, New Jersey Institute of Technology, Newark, NJ USA, January, 2018.
- [33] M. Rezaeia, D.M. Warsinger, J.H. Lienhard V, W.M. Samhabera, Wetting prevention in membrane distillation through superhydrophobicity and recharging an air layer on the membrane surface, J. Membr. Sci. 530 (2017) 42–52.
- [34] D. Singh, K.K. Sirkar, Desalination of brine and produced water by direct contact membrane distillation at high temperatures and pressures, J. Membr. Sci. 389 (2012) 380–399.
- [35] N. G. P. Chew, S. Zhao, C. Malde, R. Wang, Polyvinylidene fluoride membrane modification via oxidant-induced dopamine polymerization for sustainable directcontact membrane distillation, J. Membr. Sci., https://doi.org/10.1016/j.memsci. 2018 05 035